Check for updates

N and P-type zwitterion gated organic field effect transistors†

Jasleen Kaur, Harsimrat Kaur and Loren G. Kaake ⓘD *

Low voltage operation in organic field effect transistors (OFETs) requires dielectric materials with extremely large capacitance. We explored a novel zwitterion-based dielectric material prepared using 4-(3-Butyl-1-imidazolio)-1-butanesulfonate (ZI) in a poly(vinyl alcohol) (PVA) polymer matrix. P-type OFET devices were fabricated with poly(3-hexylthiophene-2,5-diyl) (P3HT), their performance was found to be strongly humidity dependent with humidified devices producing roughly the same current at a voltage nearly 30 times lower than devices tested under an inert atmosphere. N-type OFETs based on poly{[N,N'-bis(2-octyldodecyl)napthlene-1,4,5,8-bis(dicarboximide)-2,6-diyl]-*alt*-5,5'-(2,2'-bithiophene)} (P(NDI2OD-2T)) also showed improved current levels in humidified devices, but possessed a low on/off ratio. Impedance measurements of the dielectric film showed a marked increase in the magnitude and frequency response of the capacitance with increasing humidity. The process can be modelled in terms of a single rate-limiting process using the Havriliak–Negami equation. Infrared spectroscopy was used to further examine the intermolecular interactions responsible for the humidity-dependent capacitance. Changes were observed in the spectrum of PVA with ZI inclusion and with respect to humidity. We hypothesize that the ZI molecules rotate in response to an applied field and that rotation is inhibited by strong intermolecular interactions between ZI molecules and the polymer matrix under dry conditions. This hypothesis also can be used to rationalize the low on/off ratio of the P(NDI2OD-2T) transistors. In sum, we demonstrate a material with capacitance values approaching those of an electrostatic double layer and demonstrated that local intermolecular interactions are central to understanding material behavior.

Introduction

Organic field effect transistors (OFETs) are targeted for diverse applications including flexible displays,[1–3] sensors,[4–7] smart tags,[8,9] and integrated circuits.[10,11] Printing techniques can be employed to create circuitry based on OFET components by taking advantage of their solution processability with the use of printing techniques offering a cost advantage relative to vacuum deposition techniques.[12,13] The driving voltage of fully printed circuitry must rely on printed components like radio frequency identification (RFID) technology, printed batteries and/or supercapacitors.[14,15] This places stringent requirements on the magnitude of the voltage available to power devices. In OFETs, operational voltage is most strongly controlled by the properties of the dielectric.[16] As such, increasing the capacitance of dielectric materials for use in printed electronics is a topic of longstanding interest.[17]

Polymers like polystyrene, poly(methyl methacrylate) (PMMA), and CYTOP[17,18] are commonly used dielectric materials in OFETs. These materials act approximately as linear dielectric materials with a capacitance that is directly proportional to the dielectric constant and inversely proportional to film thickness. As such, achieving large values of the capacitance typically requires very thin films, often on the order of several nm. Despite the use of surface chemistry to address the issue,[19] creating ultrathin films using conventional printing techniques remains a challenge. In addition, larger area devices frequently suffer from gate leakage due to dielectric non-uniformity.[20,21] Alternatively, the high capacitance created at the electrolyte interface can be leveraged in this context with electrolyte dielectrics (polymer electrolytes and ion gels) frequently used to create organic thin film transistors (OTFTs) that exhibit low voltage operation while being robust to small variations in dielectric film thickness.[22]

Electrolyte dielectric materials offer a large capacitance that is largely independent of film thickness because the mobile ions in the dielectric are primarily responsible for their dielectric properties. At metal/dielectric interfaces, the formation of an electrostatic double layer leads to capacitance values of approximately 10 μF cm^{-2}. However, polymer semiconductors

Department of Chemistry, Simon Fraser University, 8888 University Dr. Burnaby, BC, Canada V5A 1S6. E-mail: lkaake@sfu.ca

are often permeable to ions,[23,24] leading to the intercalation of ions into the semiconductor bulk, creating organic electrochemical transistors (OECTs). Although these devices possess the benefits of high currents and low operating voltages,[25] the motion of ions can often limit the rate of transistor switching.[26,27] This limitation can be overcome to some degree by blending ionic liquids with organic semiconductors.[28] However, mobile ions present in the semiconductor is not ideal, in some cases compromising the properties of thin film transistors.[27,29] Polyelectrolytes such as poly(styrene sulfonic acid) are also reported for successfully driving OFETs at lower voltages.[30,31] In these devices, often called electrolyte gated organic field effect transistors (EGOFETs), an electrostatic double layer is formed between the polyanion and the polymer semiconductor. Unfortunately, this approach does not work in reverse bias, as the mobile ions necessary for the function of polyelectrolyte dielectric materials can dope the bulk of the polymer semiconductor.[32]

In order to create dielectric materials with a capacitance approaching that of an electrostatic double layer without the use of mobile ions, we explored a zwitterion-based electrolyte dielectric material. Zwitterions have an overall charge neutral structure with a covalently tethered anion and cation.[33] In contrast to their ionic liquid counterparts, zwitterions do not migrate under a potential gradient.[34,35] This approach has been employed by other groups with some success revealing high dielectric constants.[36] However, most zwitterions at room temperature are crystalline solids, with their dipole moments orienting in an antiparallel fashion, cancelling their dipole moments and limiting their dielectric behavior.[37] As such, obtaining liquid zwitterion samples at room temperature remains an ongoing challenge.[35,38,39] A zwitterionic copolymer has been studied in OFET devices as a dielectric material, using humidity to plasticize the film, allowing the zwitterionic groups to reorient in an applied field.[40] Above a relative humidity (RH) of 35% an operating voltage of 5–15 V was demonstrated.

It is also important to differentiate zwitterionic dielectric materials from other reports which mix zwitterions with mobile ions to increase the transport rate of the electrolyte. These approaches still employ mobile ions, opening them to the problems associated with conventional electrolyte dielectric materials in the context of OFETs. In alternative contexts, however, this approach has shown promise. For example, Yoshizawa et al. introduced an equimolar mixture of a zwitterion and Li salt with low melting temperature for Li^{+} ion transport.[41] They also reported a polymer gel electrolyte by mixing neutral perfluorinated polymer with zwitterion/Li-salt system.[42] Following that, zwitterions have been extensively reported in systems containing ionic liquids or Li salts as additives,[43–45] in polymer gels electrolytes,[46,47] and single ion conducting polyelectrolytes.[48–50] Further in polymeric form, ion gels prepared via in situ polymerization of zwitterion in the ionic liquid[51–53] and zwitterionic gel electrolyte using polyzwitterion/LiCl[54] are reported for energy storage applications.

In this work, we assessed the use of molecular zwitterion for room temperature dielectric in OFETs. By blending commercially available 4-(3-Butyl-1-imidazolio)-1-butanesulfonate (ZI) with poly (vinyl alcohol) (PVA) smooth films could be formed. Characterization of OFETs fabricated with poly(3-hexylthiophene-2,5-diyl) (P3HT) and Poly{[N,N′-bis(2-octyldodecyl) napthlene-1,4,5,8-bis(dicarboximide)-2,6-diyl]-alt-5,5′-(2,2′-bithiophene)} (P(NDI2OD-2T)) using ZI-based dielectric films revealed humidity dependent operational voltage with humidified P3HT OFET devices operating at voltages of −1.2 V or lower (in absolute magnitude). Dielectric films show two orders of increase in capacitance on increasing relative humidity (RH) from 20 to 70%. The observed increase in capacitance can be justified by the strong alignment of ZIs in the film under applied field when liberated from strong interactions with the PVA matrix.

Materials and methods

4-(3-Butyl-1-imidazolio)-1-butanesulfonate (ZI, ≥98%), poly (vinyl alcohol) (PVA, avg. M_w = 31 000–50 000 Da; 87–89% hydrolyzed), trichloro(octadecyl)silane (OTS, ≥90%), chlorobenzene (anhydrous, 99.8%), methanol (≥99.8%), toluene (99.9%), and hydrogen peroxide (30 wt% in H₂O) were purchased from Sigma Aldrich. Regio-regular poly(3-hexylthiophene-2,5-diyl) (P3HT, avg. M_w = 27 000–45 000 Da) and Bicyclohexyl (≥99.0%) were purchased from TCI America. Poly {[N,N′-bis(2-octyldodecyl)napthlene-1,4,5,8-bis(dicarboximide)-2,6-diyl]-alt-5,5′-(2,2′-bithiophene)}, (P(NDI2OD-2T), M_n = 65 kg mol⁻¹ and M_w = 280 kg mol⁻¹) was purchased from Brilliant Matters. Quartz coated glass substrates (15 × 20 mm²) were purchased from Ossila Limited. Deposition materials, gold (Au, 99.999%) and chromium (Cr, 99.95%) from Kurt J. Lesker were provided by 4D LABS facility at Simon Fraser University. Milli-Q water used in all experiments was produced with Barnstead EASYpure II UV/VF water purification system. Fluorosurfactant (zonyl FS-300, Alfa Chemistry), N,N-dimethylformamide (DMF ≥99.8%, ACP Chemicals Inc.), sulfuric acid (ACS reagent, Fisher Scientific), and acetone (≥99.5%, Fisher Scientific) were obtained from commercial suppliers.

For the preparation of ZI-based dielectric films, first PVA was dissolved at a concentration of 100 mg mL⁻¹ in water/DMF (1 : 1 v/v) by stirring at 90 °C for 5 hours. On complete dissolution of PVA, ZI was added to the solution with ZI/PVA weight ratio = 1 : 2 and stirred at room temperature for 2 hours. ZI-PVA dielectric films were obtained from the resulting solution by either drop casting or spin coating as noted.

OFETs with ZI-PVA dielectric in bottom contact top gate configuration were fabricated on 15 × 15 mm² substrates obtained by cutting as received 15 × 20 mm² quartz coated glass pieces. Substrates were cleaned by sequential ultrasonication for 15 minutes in water, acetone, and methanol followed by drying with nitrogen. Afterwards substrates were placed in piranha solution (3 : 1 H₂SO₄/H₂O₂ v/v) for 20 minutes, rinsed with water, and dried with nitrogen. The

© 2024 The Author(s). Published by the Royal Society of Chemistry

RSC Appl. Polym., 2024, 2, 926–935 | 927

substrates were then subjected to OTS treatment for 30 minutes in 5 mM solution of OTS in bicylcohexyl,[55] rinsed sequentially with toluene and methanol followed by annealing at 180 °C for 10 minutes. The substrates were then transferred to an inert atmosphere glovebox where a spin coater and physical vapor deposition (PVD) system is located. Source and drain electrodes (5 nm Cr and 60 nm Au) were deposited on top of OTS treated substrates with a shadow mask using the PVD system defining channel length (L = 150 μm) and width (W = 3000 μm). Next for the P3HT OFETs, P3HT (10 mg mL^{-1}) solution in chlorobenzene was prepared inside the glovebox by stirring at 65 °C. The obtained solution was passed through a 0.45 μm polytetrafluoroethylene (PTFE) syringe filter. P3HT films, approximately 20 nm in thickness were deposited by spin coating at 2000 rpm for 60 s. P3HT films were then annealed at 130 °C for 1 hour inside the glovebox. Following this, the deposition of the dielectric film was carried out under ambient conditions. A fluorosurfactant (Zonyl FS 300)[30] was added to the dielectric solution described above at a concentration of 15 μL mL^{-1}. The dielectric solution was filtered through a 0.45 μm PTFE syringe filter and spin coated at 1500 rpm for 100 s. Devices were annealed at 100 °C for 20 minutes. The film thickness of the dielectric layer was determined to be 1.2 ± 0.1 μm via profilometry. The top gate electrode (Au, 60 nm) was then deposited through a shadow mask using a PVD system located inside the glovebox to complete device fabrication. For the OFETs with P(NDI2OD-2T),[56] P(NDI2OD-2T) (10 mg mL^{-1}) in chlorobenzene was prepared inside the glovebox by stirring at 70 °C. Films in the range of 35–40 nm were deposited by spin coating at 2000 rpm for 60 s onto the substrates with deposited source and drain electrodes as described above. Deposited films of P(NDI2OD-2T) were then annealed at 110 °C for one hour inside the glovebox. Following that, the deposition of the dielectric layer and top gate contact was done as described above. The reported thicknesses of semiconducting and dielectric films were determined using Bruker Dektak XT profilometer. For the characterization of P3HT and P(NDI2OD-2T) OFETs under dry conditions, output and transfer characteristics were studied using Keithley 2634B Source Meter and Keithley 6485 Picoammeter inside the glovebox at a sweep rate of 200 mV s^{-1}. Electrical characteristics of devices under humid conditions were performed on an Agilent B1500A Semiconductor device Analyzer at a sweep rate of 200 mV s^{-1} either with recorded ambient RH = 70% or by humidifying devices for 10 minutes inside a humidity chamber prior to the measurement.

Metal–insulator–metal capacitors were prepared on 15 × 15 mm^2 quartz coated glass substrates. The substrates were cleaned by ultrasonication in water, acetone, and methanol sequentially (15 minutes each) followed by drying with nitrogen. For the final cleaning step, dried substrates were placed in piranha solution for 20 minutes and were rinsed with water followed by drying with nitrogen. Cleaned substrates were transferred to an inert atmosphere glovebox where 5 nm of Cr followed by 70 nm of Au were deposited via PVD. ZI-PVA dielectric films were deposited under ambient conditions by spin

coating the dielectric solution described above. A 0.45 μm PTFE syringe filter was used to filter the dielectric solution. The solution was then spin coated onto the substrates deposited with Cr–Au at 1500 rpm for 60 s. The spun films were then annealed at 100 °C for 20 minutes following which samples were transferred to the glovebox for deposition of the top contact. The thickness of ZI-PVA dielectric film was determined to be 1.2 ± 0.1 μm. Top contact (Au, 70 nm) deposited by PVD through a shadow mask in the shape of a circle with diameter of 7 mm. Control devices using PVA thin films were prepared by spin coating PVA solution at a concentration of (100 mg mL^{-1} in water/DMF). Films were 0.9 ± 0.1 μm in thickness. Metal–insulator–metal capacitors were measured using a Solartron Impedance Analyzer and humidified for 10 minutes before collecting the measurement in a humidity chamber. The reported thicknesses of ZI-PVA and PVA films were measured by Bruker Dektak XT profilometer.

Differential scanning calorimetry (DSC) measurements on pure ZI powder, ZI-PVA film, and PVA film samples were performed using PerkinElmer 6000 DSC at a heating rate of 5 °C min^{-1}. Film samples were obtained by drop casting 0.8 mL ZI-PVA or PVA solution on a clean 2.54 × 7.62 mm^2 glass slide followed by drying overnight and annealing afterward at 100 °C for one hour inside an inert atmosphere glovebox. The sample preparation procedure was carried out at RH ≤ 30%.

Infrared spectroscopy (IR) measurements on pure ZI powder, ZI-PVA film, and PVA film samples were recorded at RH < 20% using a PerkinElmer infrared spectrometer at a resolution of 4 cm^{-1}. Additionally, the measurement for a ZI-PVA film humidified at RH = 70% for 30 minutes was taken using the same scan parameters.

Results and discussion

To evaluate the performance of a ZI-based dielectric, OFETs in a bottom contact top gate configuration were fabricated. The ZI (shown in Fig. 1a) was blended with PVA as described above to obtain ZI-PVA dielectric films. Representative output and transfer curves for P3HT OFETs collected under dry conditions inside an inert atmosphere glovebox at a sweep rate of 200 mV s^{-1} are shown in Fig. 1b and c. The output curves (Fig. 1b) show expected p-type switching with an increase in magnitude of output current (I_D) upon increasing the magnitude of the gate voltage (V_G). The device shows a maximum current ≈180 nA in magnitude for drain voltage (V_D) = V_G = −30 V. Additionally, hysteresis was observed between forward and reverse sweep in the output curves which is partly reduced on increasing V_G. The threshold voltage (V_T) and hole mobility values (μ) were extracted from the forward sweep of the transfer curve (I_D–V_G) at V_D = −30 V (Fig. 1c) and are 20 V and 0.004 cm^2 V^{-1} s^{-1} respectively. The voltages required to operate the transistor are somewhat lower than a comparable device using poly(methyl methacrylate) (PMMA) as the dielectric material (Fig. S1†), however, devices still require moderate voltages to turn on. This indicates that the inclusion of ZI mole-
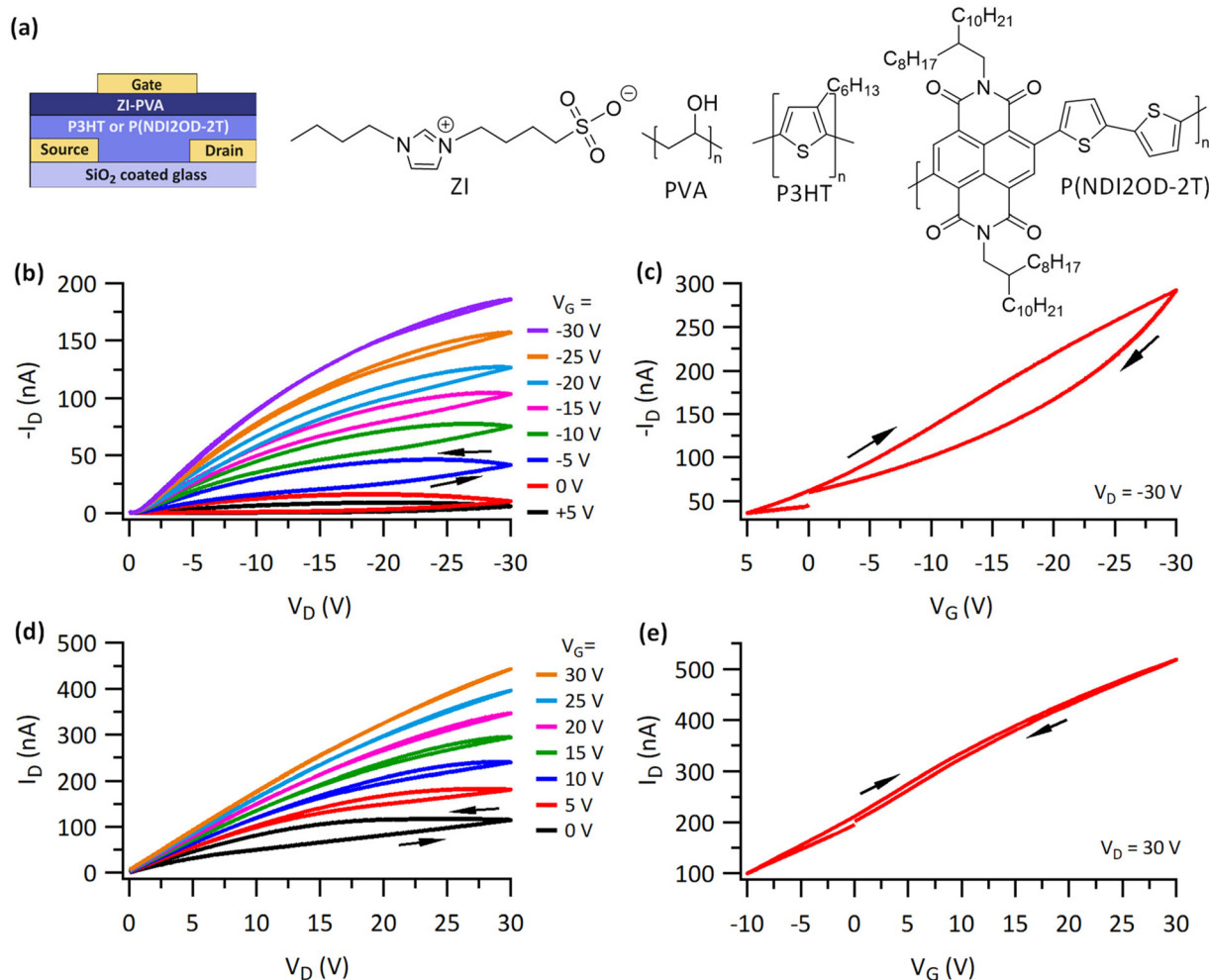
Fig. 1 OFETs with ZI-PVA dielectric under dry conditions. (a) Schematic of the fabricated OFET and chemical structures of materials used in the study. (b) Output curves of a P3HT device at different applied voltages at gate ranging from +5 to −30 V (c) transfer curve of the same device at V_D = −30 V. (d) Output curves of a P(NDI2OD-2T) OFET (e) transfer curve of the same device at V_D = 30 V. The direction of the hysteresis is indicated with the arrows.

cules into the dielectric has a beneficial effect, increasing the dielectric constant of the film, but the overall voltages required for transistor operation remain too high for many applications in printed applications.

The output and transfer curves (Fig. 1b and c) show marked hysteresis with a lower current on the back sweep in the transfer curve and a higher current on the back sweep in the output curve. Hysteresis can be caused by charge trapping near the semiconductor/dielectric interface, mobile ions in the semiconductor, ferroelectricity in the dielectric, and mobile ions in the dielectric.[57] A lower current on the back sweep in the transfer curve is typically associated with charge trapping processes or mobile ions in the semiconductor.[58] Devices using a PMMA dielectric show very little hysteresis, pointing towards the dielectric as the cause of the hysteresis observed in Fig. 1b and c. Owing to the large dipole moment of the ZI molecules, the formation of Froelich polarons is likely,[59] with this process possibly being exacerbated by a degree of ferroelectric behavior

in the dielectric material, leading to charge trapping. This is supported by the appearance of somewhat large off-currents at positive V_G. For comparison, P3HT OFETs with a PVA dielectric were measured under same dry conditions (Fig. S2†). They showed a lower off current, a higher on current, but device yield was lower and frequently displayed a higher leakage current relative to devices with ZI-PVA as a dielectric.

The output curves for P(NDI2OD-2T) based OFETs were measured under dry conditions at a sweep rate of 200 mV s⁻¹. Fig. 1d shows representative device performance characterized by modulation of I_D with V_G. A charge carrier mobility of 0.005 cm² V⁻¹ s⁻¹ was extracted from the transfer curve (Fig. 1e). This value is higher than P3HT devices and is presumably the reason for higher on current in P(NDI2OD-2T) device. The transfer curve (Fig. 1e) also reveals a high off-current with a smaller hysteresis as compared to the P3HT OFET (Fig. 1c). The observed on–off ratio is also low, consistent with a large negative threshold voltage. This behavior is

© 2024 The Author(s). Published by the Royal Society of Chemistry

RSC Appl. Polym., 2024, **2**, 926–935 | **929**

likely the result of a degree of incipient polarization, favoring electron accumulation in the absence of applied voltage. To investigate the role of ZI in the observed behavior P(NDI2OD-2T) OFETs fabricated with a PVA dielectric were also measured. Device yield was extremely poor, suggesting that PVA is a poor dielectric material for n-type devices, and that the ZI exerts an important, beneficial influence on their performance. These results are consistent with an accumulation of ZI molecules at the semiconductor/dielectric interface.

To examine device operation under ambient conditions, devices were humified at 70% RH before electrical characterization. Devices are improved by virtually every available metric. Output curves for P3HT OFETs (Fig. 2a) showed lower operating voltage (V_G = 0 to −1.2 V, V_D = 0 to −2 V) with a current of 200 nA in magnitude at V_G = −1.2 and V_D = −2 V. Improved saturation behavior was also observed. The transfer curve in Fig. 2b shows a threshold voltage of −0.4 V with a mobility value of 0.09 cm^2 V^{-1} s^{-1}, approximately a 20-fold improvement relative to dry devices. Hysteresis in both the output and transfer curves is also lessened, as is the off current, resulting in a higher on–off ratio. As a comparison, devices employing a humidified PVA dielectric were also measured (Fig. S3†). They required higher operating voltages and showed larger hysteresis in their transfer curves relative to devices with a humidified ZI-PVA dielectric material. Representative output and transfer curves for P(NDI2OD-2T) OFET devices characterized following humidification are shown in Fig. 2c and d. The devices showed improved saturation, which is evident from output curves (Fig. 2c), however, current for lower voltages remained low when compared to P(NDI2OD-2T) based devices measured under dry conditions. This can be understood in general considering the sensitivity of P(NDI2OD-2T) to oxygen and water. The transfer of electrons from the polymer to the hydroxide ion in the presence of oxygen and water leads to electron trapping causing shifts in the threshold voltages.[60] Further, the interaction of oxygen with naphthalene diimide in P(NDI2OD-2T) can be manifested by a decrease in mobility and the I_{on}/I_{off} ratio of the device.[60,61] We note that low voltage operation in humidified P3HT OFETs does not arise from electrochemical doping of P3HT film as suggested by cyclic voltammetry measurements of P3HT in a ZI solution (Fig. S4†).

To investigate the underlying mechanism for the improvement in P3HT OFET devices performance with increasing humidity, metal–insulator–metal capacitors were prepared. ZI-PVA films were spin coated onto gold coated quartz substrates and a gold top contact was formed via thermal vapor deposition. The frequency dependent dielectric properties were measured at an AC voltage of 0.1 V at varying humidity levels (Fig. 3a). At the highest frequencies, the capacitance of
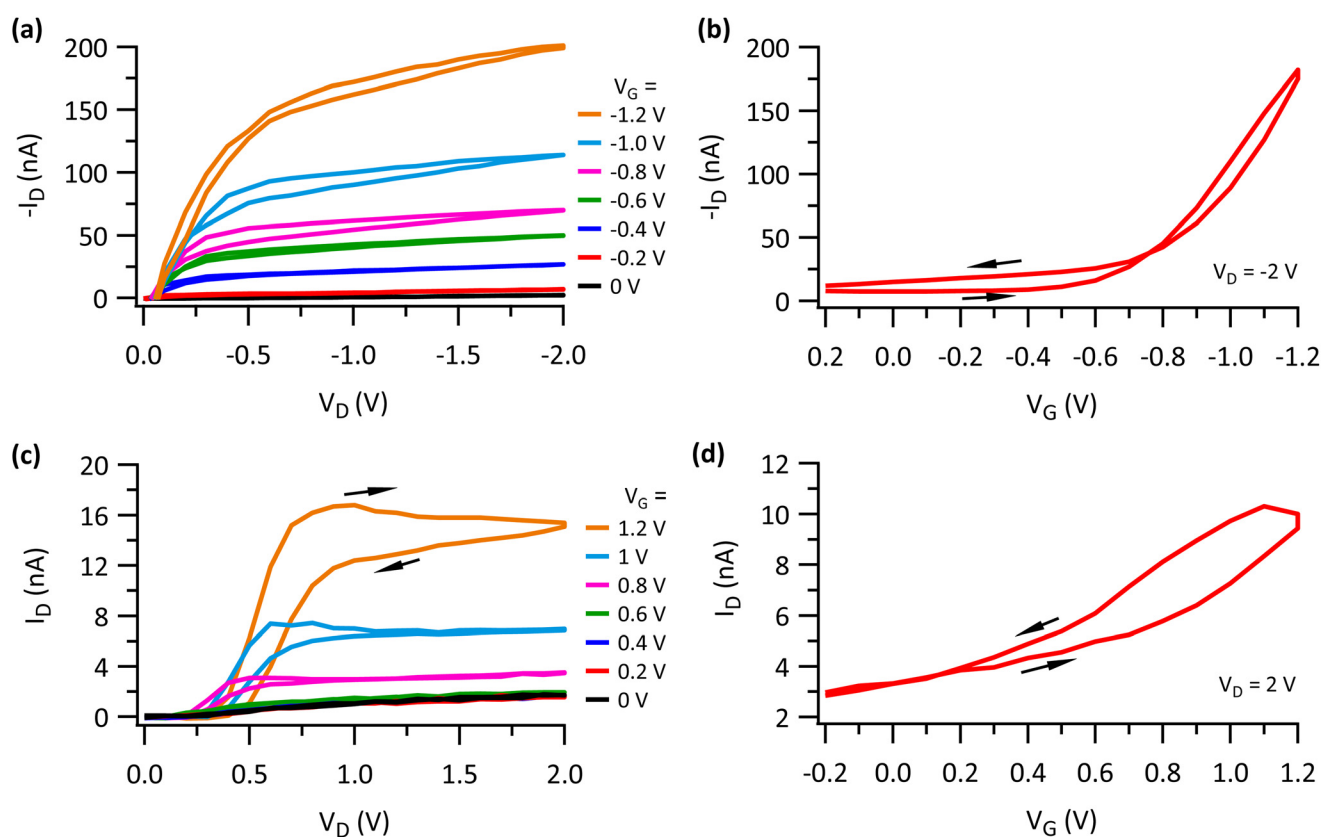

Fig. 2 OFETs with ZI-PVA dielectric measured by humidification at relative humidity of 70%. (a and b) Output and transfer curves of a humidified P3HT device. (c and d) Output and transfer curves of a humidified P(NDI2OD-2T) device. The direction of the hysteresis is shown by the arrows.
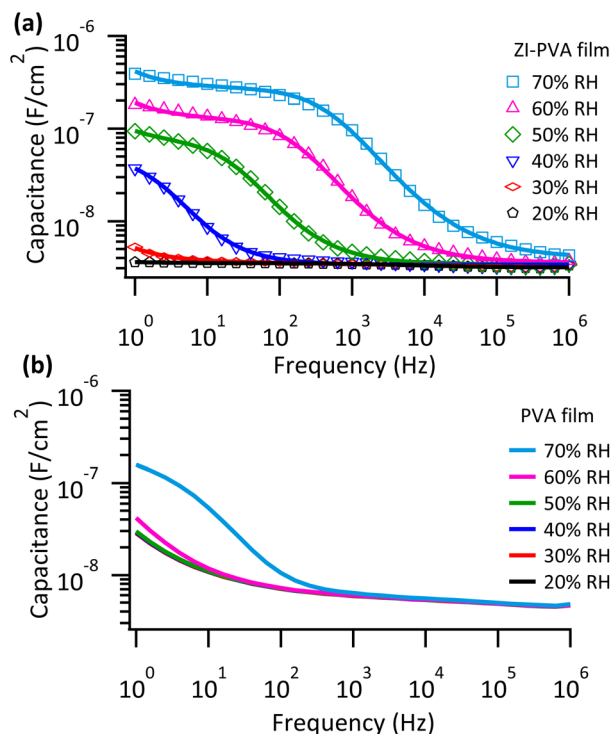
Fig. 3 Frequency dependent capacitance response. (a) Frequency dependent areal capacitance at RH ranging from 20 to 70% for a ZI-PVA dielectric film. Fit to Havriliak–Negami model shown in solid lines (b) areal capacitance *versus* frequency of a PVA film at different RH.

the device is independent of humidity, reaching an asymptote of approximately 3 nF cm^{-2}, consistent with the order of magnitude expected of a linear dielectric material. At lower frequencies, a dramatic increase in capacitance is observed with increases in RH. Specifically, the capacitance increases by two orders of magnitude upon increasing RH from 20% to 70%. In addition, improvements in the frequency response are observed, with higher RH being correlated with larger capacitance values at higher frequencies. This observation is strongly correlated with improvements observed in the operating voltage of P3HT OFETs with ZI-PVA dielectric. As a comparison, samples of PVA without ZI (Fig. 3b) show little to no improvement in capacitance when RH increases from 20% to 60% with only a slight increase in RH 70% at lower frequencies. The results strongly suggest that the properties of ZI molecules in the film play an important role in the observed device improvements. Interestingly, the capacitance of ZI-PVA films is also influenced by the applied voltage, with increases in the low frequency capacitance being correlated with increasing voltage as predicted by Eyring (Fig. S6†).[62]

In order to quantify the changes in the dielectric behavior of ZI containing film, the capacitance *versus* frequency response was fit with the Havriliak Negami eqn (1) [63,64] with fits shown in solid lines in Fig 3a.

$$C(\nu) = C_\infty + \frac{(C_0 - C_\infty)}{(1 + (i2\pi\nu\tau)^\beta)^\gamma} + \frac{1}{R_\nu} \quad (1)$$

The fitting parameters C_∞ and C_0 are capacitances at the high and low frequency limit, τ is the relaxation time, β and γ are related to the distribution of relaxation times, and R is the parallel leakage resistance. In the fit, a parallel leakage resistance was included. However, the calculated leakage resistance was high (> 1 MΩ) indicating very little leakage current in the device. Extracted fit parameters are available in Table S1.† The quality of the fit suggests that a single, spectrally broadened mechanism is responsible for high capacitance device behavior. In addition, the capacitance of ZI-PVA dielectric film at higher humidities is very high, resembling that of an electrostatic double layer.[21] We therefore hypothesize that humidity softens the film, allowing reorientation of ZIs in the direction of the applied field, yielding a large electric field at the dielectric/semiconductor interface.

This hypothesis is supported by Peng *et al.* who investigated a zwitterionic gel electrolyte, showing that zwitterionic groups orient under an applied electric field.[54] This orientation would allow them to cancel out the electric field in the material bulk, creating necessary conditions for the accumulation of large electric fields at the material interface. The high capacitance leads to a lowering of operating voltage and an increase in charge carrier mobility as a result of a high charge carrier density.[65]

In addition to the hypothesis that high capacitance behavior is linked to correlated rotations of the ZI molecules, several counter-hypotheses were also examined. These include the motion of charged species, either in the form of mobile impurity ions or protons. The possibility of mobile ions dominating thin film behavior was ruled out by adding NaCl to PVA instead of ZI. The concentration of NaCl was chosen by calculating the percentage of ionic impurities in commercially available ZI used in these experiments. Capacitance *versus* frequency response of PVA and NaCl-PVA film at RH = 50% is shown in Fig. S7.† It is very low, allowing us to rule out capacitance due to ionic impurities. On the other hand, proton conduction is vital to the properties of polyelectrolytes like poly (styrene sulfonic acid).[30] Indeed, mixtures of different molecular zwitterions and bis((trifluorosulfonyl)amide) (HTFSI) have been reported for proton transport applications.[66,67] However, our system was measured and found to be pH neutral. Owing to the low concentration of protons at neutral pH, we rule out this contribution as the dominant factor in establishing the high capacitance of our ZI containing film. This hypothesis agrees with the report of Shen *et al.* who indicate that the capacitive response of zwitterionic copolymer films is produced mainly due alignment of pendant zwitterionic groups.[40]

To further understand the mechanism that underlies the humidity dependent capacitance, we performed differential scanning calorimetry (DSC) on samples handled at RH ≤ 30%. One hypothesis is that the antiparallel molecular alignments typical of zwitterion crystals lead to a cancellation of their dipole moments.[38] In this scenario, humidification of the film would lead to a disruption of ZI crystals, facilitating their rotation in an applied field. Fig. 4a shows the results of DSC
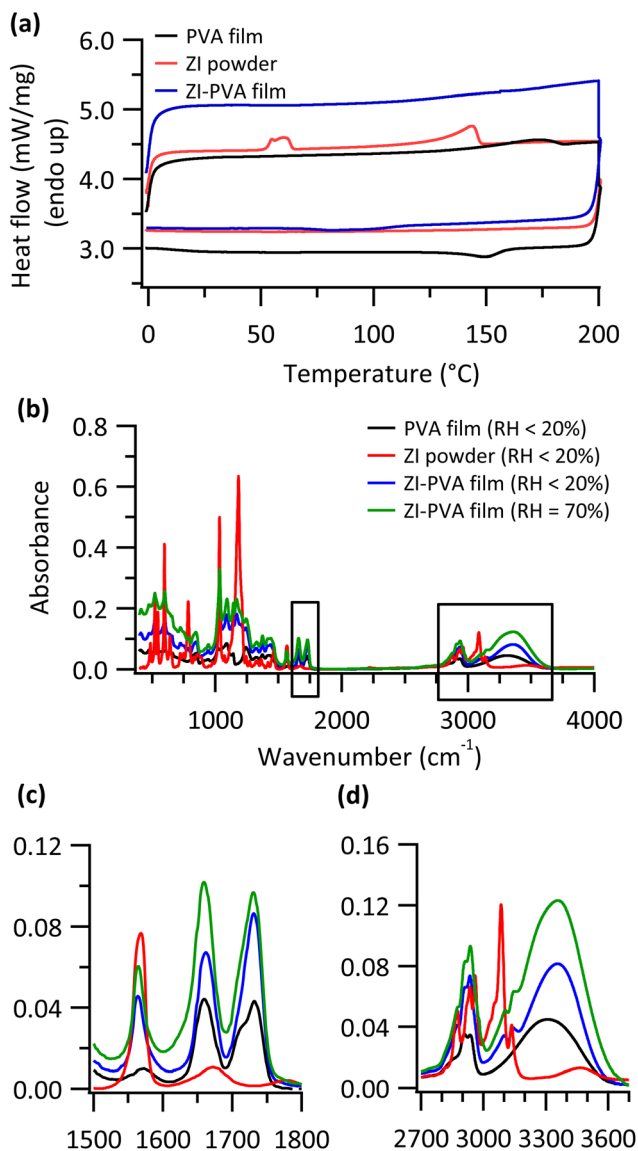
Fig. 4 DSC and IR measurements. (a) DSC traces collected at a scan rate 5 °C min⁻¹ for a ZI-PVA film, a PVA film, and a pure ZI powder, samples handled at RH ≤ 30%. First heating and cooling cycle is shown. (b) IR spectra comparing a ZI-PVA film, a PVA film, and a pure ZI powder, all handled at RH < 20%, and ZI-PVA film humidified at RH = 70%. (c) IR spectra of CO stretching region and (d) IR spectra of OH stretching region expanded from b for clarity.

scans for pure ZI powder, a ZI-PVA film, and a PVA film. The melting peak for a pure ZI powder can be seen 143.7 °C with an additional crystal reorganization peak around 60 °C, consistent with literature reports.[36,68] These peaks are missing from the reverse scan, with ZI exhibiting pronounced super-cooling behavior. This supercooling behavior is also clearly observed in a second heating and cooling scan (Fig. S8†). In the PVA film, a broad endothermic feature was observed around 160–180 °C. This feature is related to the melting of PVA.[69] Importantly, the DSC trace of ZI-PVA film does not show melting peaks related to pure ZI. This indicates that pure ZI crystals are not present in the blended material presumably

because of their interactions with PVA.[47] Thus, we conclude that ZI is well-dispersed in PVA, even in dry films. Therefore, the role of increasing RH is not to disrupt ZI crystals and lower the strength of intermolecular interactions which hinder their rotation.

Alternatively, interactions between ZI and PVA, important in creating a smooth and homogeneous film, are responsible for the hindered rotation at low humidities. To evaluate this hypothesis, we collected infrared spectra of both dry (handled at RH < 20%) and deliberately humidified thin film samples. Fig. 4b shows the full spectral range, with regions of interest highlighted in Fig. 4c and d. In the carbonyl (CO) stretching region (Fig. 4c), two peaks were observed for acetate group present in non-hydrolyzed PVA. The maxima for these peaks are shifted for ZI-PVA films with additional changes in peak shape being observed. This confirms an interaction between non-hydrolyzed PVA monomer units and ZI.

Fig. 4c also shows the effect of humidifying the film, with pronounced spectral changes being observed. This demon-strates that the interactions between the ZI and non-hydro-lyzed PVA are affected by the presence of water, presumably facilitating the rotation of ZIs in an electric field. An examin-ation of the OH stretching region (Fig. 4d) suggests that ZI is also associated with hydrolyzed PVA monomer units. A blue shift is observed in the peak maxima for ZI-PVA film compared to PVA. However, this shift decreases with increasing humidity, forming a low energy shoulder in the humidified ZI-PVA film. We therefore conclude that interactions between the OH of PVA and hygroscopic SO_3^- functional groups also can inhibit the rotation of ZIs. Increasing humidity can interfere with these interactions and facilitate the rotation of the ZI in the presence of an applied field, allowing the establishment of a large interfacial electric field and a large value of device capacitance.

This description can also be used to explain the negative threshold voltage and large on-currents in P(NDI2OD-2T) OFET devices. Interactions between the SO_3^- functional groups and PVA impart a preferential alignment of the ZI molecules. The SO_3^- functional groups are aligned towards the dielectric interior through their interactions with PVA, pointing the positively charged imidazolium groups toward the semi-conductor interface. This partial positive charge would impart a positive potential at the dielectric/semiconductor interface, stabilizing electronic charge carriers in the P(NDI2OD-2T) polymer, and leading to a negative threshold voltage. Taken in sum, the results indicate that in a ZI-PVA blend, there exists an important interplay regarding the interactions between ZI molecules and polymer matrix. Too little interaction and the ZIs will not dissolve well, too strong of an interaction and this interaction can inhibit ZI rotation.

Conclusions

To create a dielectric material with large capacitance support-ing both p-type and n-type OFETs, we investigated a zwitter-

ion-based dielectric material prepared by blending 4-(3-Butyl-1-imidazolio)-1-butanesulfonate (ZI) with PVA. Dry p-type and n-type OFETs fabricated with P3HT, and P(NDI2OD-2T) operated at 10 s of volts. Upon humidifying the devices, P3HT OFETs operated with $|V_G| < |-1.2\text{ V}|$, also showing higher mobility and a reduction of hysteresis. OFETs with P(NDI2OD-2T) also showed improved characteristics, however, these were masked to some extent by side reactions with water and oxygen. The role of humidity in improving the performance of P3HT OFETs is more clearly understood by studying the capacitance response of ZI-PVA dielectric film. Impedance spectroscopy shows a strong humidity dependence, with an increase in thin film capacitance by two orders in magnitude upon increasing RH from 20 to 70%. Impedance data were fit with a Havriliak–Negami model employing a single, spectrally broadened time constant, suggesting that a single mechanism is primarily responsible for the observed increase in capacitance with humidity. The results suggest that ZI molecules rotate in an applied electric field, providing a large electric field at the electrode interface, and thus a large thin film capacitance. Further investigation of molecular level ZI–ZI and ZI–polymer interactions in the dielectric film by DSC and IR revealed that ZI–polymer interactions in dry films hinder ZI reorientation under an applied electric field. These interactions can be overcome by humidity leading to easy orientation and increased capacitance response.

Author contributions

The manuscript was written through contributions of all authors. All authors have given approval to the final version of the manuscript.

Data availability

Additional data regarding materials, the performance of P3HT OFETs employing a PMMA dielectric, the performance of P3HT OFETs employing a PVA dielectric, cyclic voltammetry of P3HT in solutions containing zwitterions, details on data fitting with the Havriliak–Negami model, the effect of voltage on frequency-dependent capacitance, the capacitance response of impurities in PVA, and thermal analysis can be found in the electronic ESI.† Data can be made available upon request.

Conflicts of interest

There are no conflicts to declare.

Acknowledgements

References

1 Z. Bao and X. Chen, Flexible and Stretchable Devices, *Adv. Mater.*, 2016, **28**, 4177–4179.

2 K. Liu, B. Ouyang, X. Guo, Y. Guo and Y. Liu, Advances in flexible organic field-effect transistors and their applications for flexible electronics, *npj Flexible Electron.*, 2022, **6**, 1–19.

3 Z.-L. Gong, Y. Guo and Y.-W. Zhong, Advances in organic field-effect transistors based on metal–organic coordination materials and applications, *Mater. Chem. Front.*, 2023, **7**, 6281–6304.

4 W. Gao, H. Ota, D. Kiriya, K. Takei and A. Javey, Flexible Electronics toward Wearable Sensing, *Acc. Chem. Res.*, 2019, **52**, 523–533.

5 G. Schwartz, B. C.-K. Tee, J. Mei, A. L. Appleton, D. H. Kim, H. Wang and Z. Bao, Flexible polymer transistors with high pressure sensitivity for application in electronic skin and health monitoring, *Nat. Commun.*, 2013, **4**, 1859.

6 H. Li, W. Shi, J. Song, H.-J. Jang, J. Dailey, J. Yu and H. E. Katz, Chemical and Biomolecule Sensing with Organic Field-Effect Transistors, *Chem. Rev.*, 2019, **119**, 3–35.

7 J. Sun, G. Zhao, M. Zhang, X. Zhao, Y. Tong, Q. Tang and Y. Liu, Intrinsically stretchable organic field-effect transistors: progress and challenges, *J. Mater. Chem. C*, 2024, **12**, 6011–6026.

8 E. Cantatore, T. C. T. Geuns, G. H. Gelinck, E. van Veenendaal, A. F. A. Gruijthuijsen, L. Schrijnemakers, S. Drews and D. M. de Leeuw, A 13.56 MHz RFID System Based on Organic Transponders, *IEEE J. Solid-State Circuits*, 2007, **42**, 84–92.

9 V. Subramanian, P. C. Chang, J. B. Lee, S. E. Molesa and S. K. Volkman, Printed organic transistors for ultra-low-cost RFID applications, *IEEE Trans. Compon. Packag. Technol.*, 2005, **28**, 742–747.

10 K.-J. Baeg, M. Caironi and Y.-Y. Noh, Toward Printed Integrated Circuits based on Unipolar or Ambipolar Polymer Semiconductors, *Adv. Mater.*, 2013, **25**, 4210–4244.

11 H. Matsui, Y. Takeda and S. Tokito, Flexible and printed organic transistors: From materials to integrated circuits, *Org. Electron.*, 2019, **75**, 105432.

12 F. C. Krebs, All solution roll-to-roll processed polymer solar cells free from indium-tin-oxide and vacuum coating steps, *Org. Electron.*, 2009, **10**, 761–768.

© 2024 The Author(s). Published by the Royal Society of Chemistry

RSC Appl. Polym., 2024, **2**, 926–935 | **933**

13 R. R. Søndergaard, M. Hösel and F. C. Krebs, Roll-to-Roll fabrication of large area functional organic materials, *J. Polym. Sci., Part B: Polym. Phys.*, 2013, **51**, 16–34.

14 Z. Wu, Y. Wang, X. Liu, C. Lv, Y. Li, D. Wei and Z. Liu, Carbon-Nanomaterial-Based Flexible Batteries for Wearable Electronics, *Adv. Mater.*, 2019, **31**, 1800716.

15 D. P. Dubal, N. R. Chodankar, D.-H. Kim and P. Gomez-Romero, Towards flexible solid-state supercapacitors for smart and wearable electronics, *Chem. Soc. Rev.*, 2018, **47**, 2065–2129.

16 A. Facchetti, M.-H. Yoon and T. J. Marks, Gate Dielectrics for Organic Field-Effect Transistors: New Opportunities for Organic Electronics, *Adv. Mater.*, 2005, **17**, 1705–1725.

17 B. Wang, W. Huang, L. Chi, M. Al-Hashimi, T. J. Marks and A. Facchetti, High-k Gate Dielectrics for Emerging Flexible and Stretchable Electronics, *Chem. Rev.*, 2018, **118**, 5690–5754.

18 B. Nketia-Yawson and Y.-Y. Noh, Recent Progress on High-Capacitance Polymer Gate Dielectrics for Flexible Low-Voltage Transistors, *Adv. Funct. Mater.*, 2018, **28**, 1802201.

19 S. P. Senanayak, V. K. Sangwan, J. J. McMorrow, K. Everaerts, Z. Chen, A. Facchetti, M. C. Hersam, T. J. Marks and K. S. Narayan, Self-Assembled Nanodielectrics for High-Speed, Low-Voltage Solution-Processed Polymer Logic Circuits, *Adv. Electron. Mater.*, 2015, **1**, 1500226.

20 J. Li, W. Tang, Q. Wang, W. Sun, Q. Zhang, X. Guo, X. Wang and F. Yan, Solution-processable organic and hybrid gate dielectrics for printed electronics, *Mater. Sci. Eng., R*, 2018, **127**, 1–36.

21 W. Cai, J. Wilson and A. Song, Present status of electric-double-layer thin-film transistors and their applications, *Flexible Printed Electron.*, 2021, **6**, 043001.

22 S. H. Kim, K. Hong, W. Xie, K. H. Lee, S. Zhang, T. P. Lodge and C. D. Frisbie, Electrolyte-Gated Transistors for Organic and Printed Electronics, *Adv. Mater.*, 2013, **25**, 1822–1846.

23 J. Lee, M. J. Panzer, Y. He, T. P. Lodge and C. D. Frisbie, Ion Gel Gated Polymer Thin-Film Transistors, *J. Am. Chem. Soc.*, 2007, **129**, 4532–4533.

24 J. Lee, L. G. Kaake, J. H. Cho, X.-Y. Zhu, T. P. Lodge and C. D. Frisbie, Ion Gel-Gated Polymer Thin-Film Transistors: Operating Mechanism and Characterization of Gate Dielectric Capacitance, Switching Speed, and Stability, *J. Phys. Chem. C*, 2009, **113**, 8972–8981.

25 J. Rivnay, S. Inal, A. Salleo, R. M. Owens, M. Berggren and G. G. Malliaras, Organic electrochemical transistors, *Nat. Rev. Mater.*, 2018, **3**, 1–14.

26 P. R. Paudel, J. Tropp, V. Kaphle, J. D. Azoulay and B. Lüssem, Organic electrochemical transistors – from device models to a targeted design of materials, *J. Mater. Chem. C*, 2021, **9**, 9761–9790.

27 Y. Lei, P. Li, Y. Zheng and T. Lei, Materials design and applications of n-type and ambipolar organic electrochemical transistors, *Mater. Chem. Front.*, 2024, **8**, 133–158.

28 X. Wu, A. Surendran, J. Ko, O. Filonik, E. M. Herzig, P. Müller-Buschbaum and W. L. Leong, Ionic-Liquid Doping Enables High Transconductance, Fast Response Time, and High Ion Sensitivity in Organic Electrochemical Transistors, *Adv. Mater.*, 2019, **31**, 1805544.

29 L. Kergoat, B. Piro, M. Berggren, G. Horowitz and M.-C. Pham, Advances in organic transistor-based bio-sensors: from organic electrochemical transistors to electrolyte-gated organic field-effect transistors, *Anal. Bioanal. Chem.*, 2012, **402**, 1813–1826.

30 E. Said, X. Crispin, L. Herlogsson, S. Elhag, N. D. Robinson and M. Berggren, Polymer field-effect transistor gated via a poly(styrenesulfonic acid) thin film, *Appl. Phys. Lett.*, 2006, **89**, 143507.

31 E. Said, O. Larsson, M. Berggren and X. Crispin, Effects of the Ionic Currents in Electrolyte-gated Organic Field-Effect Transistors, *Adv. Funct. Mater.*, 2008, **18**, 3529–3536.

32 D. Rawlings, E. M. Thomas, R. A. Segalman and M. L. Chabinyc, Controlling the Doping Mechanism in Poly(3-hexylthiophene) Thin-Film Transistors with Polymeric Ionic Liquid Dielectrics, *Chem. Mater.*, 2019, **31**, 8820–8829.

33 H. Ohno, M. Yoshizawa-Fujita and Y. Kohno, Design and properties of functional zwitterions derived from ionic liquids, *Phys. Chem. Chem. Phys.*, 2018, **20**, 10978–10991.

34 F. Jesus, H. Passos, A. M. Ferreira, K. Kuroda, J. L. Pereira, F. J. M. Gonçalves, J. A. P. Coutinho and S. P. M. Ventura, Zwitterionic compounds are less ecotoxic than their analogous ionic liquids, *Green Chem.*, 2021, **23**, 3683–3692.

35 M. Yoshizawa-Fujita and H. Ohno, Applications of Zwitterions and Zwitterionic Polymers for Li-Ion Batteries, *Chem. Rec.*, 2023, **23**, e202200287.

36 W. Mei, A. J. Rothenberger, J. E. Bostwick, J. M. Rinehart, R. J. Hickey and R. H. Colby, Zwitterions Raise the Dielectric Constant of Soft Materials, *Phys. Rev. Lett.*, 2021, **127**, 228001.

37 W. Mei, A. Han, R. J. Hickey and R. H. Colby, Effect of chemical substituents attached to the zwitterion cation on dielectric constant, *J. Chem. Phys.*, 2021, **155**, 244505.

38 M. Yoshizawa-Fujita, T. Tamura, Y. Takeoka and M. Rikukawa, Low-melting zwitterion: effect of oxyethylene units on thermal properties and conductivity, *Chem. Commun.*, 2011, **47**, 2345–2347.

39 F. Makhlooghiazad, L. A. O'Dell, L. Porcarelli, C. Forsyth, N. Quazi, M. Asadi, O. Hutt, D. Mecerreyes, M. Forsyth and J. M. Pringle, Zwitterionic materials with disorder and plasticity and their application as non-volatile solid or liquid electrolytes, *Nat. Mater.*, 2022, **21**, 228–236.

40 J. Shen, S. Feng, Y. Ling, C.-C. Chang, C. Huang, X. Wu, S. Chen, J. Liu, Y. Wu and W. Huang, Responsive Zwitterionic Polymers with Humidity and Voltage Dual-Switching for Multilevel Date Encryption and Anticounterfeiting, *Chem. Mater.*, 2021, **33**, 1477–1488.

41 M. Yoshizawa, M. Hirao, K. Ito-Akita and H. Ohno, Ion conduction in zwitterionic-type molten salts and their polymers, *J. Mater. Chem.*, 2001, **11**, 1057–1062.

42 H. Ohno, M. Yoshizawa and W. Ogihara, A new type of polymer gel electrolyte: zwitterionic liquid/polar polymer mixture, *Electrochim. Acta*, 2003, **48**, 2079–2083.

43 A. Islam, J. Li, M. Pervaiz, Z.-H. Lu, M. Sain, L. Chen and X. Ouyang, Zwitterions for Organic/Perovskite Solar Cells, Light-Emitting Devices, and Lithium Ion Batteries: Recent Progress and Perspectives, *Adv. Energy Mater.*, 2019, **9**, 1803354.

44 N. Byrne, P. C. Howlett, D. R. MacFarlane and M. Forsyth, The Zwitterion Effect in Ionic Liquids: Towards Practical Rechargeable Lithium-Metal Batteries, *Adv. Mater.*, 2005, **17**, 2497–2501.

45 D. Q. Nguyen, J. Hwang, J. S. Lee, H. Kim, H. Lee, M. Cheong, B. Lee and H. S. Kim, Multi-functional zwitterionic compounds as additives for lithium battery electrolytes, *Electrochem. Commun.*, 2007, **9**, 109–114.

46 Z. H. Li, Q. L. Xia, L. L. Liu, G. T. Lei, Q. Z. Xiao, D. S. Gao and X. D. Zhou, Effect of zwitterionic salt on the electrochemical properties of a solid polymer electrolyte with high temperature stability for lithium ion batteries, *Electrochim. Acta*, 2010, **56**, 804–809.

47 Y. Yu, N. Sun, A. Wu, F. Lu and L. Zheng, Zwitterion-containing electrolytes with semi–crystalline PVDF-Co-HFP as a matrix for safer lithium-ion batteries, *J. Mol. Liq.*, 2019, **282**, 340–346.

48 C. Tiyapiboonchaiya, J. M. Pringle, J. Sun, N. Byrne, P. C. Howlett, D. R. MacFarlane and M. Forsyth, The zwitterion effect in high-conductivity polyelectrolyte materials, *Nat. Mater.*, 2004, **3**, 29–32.

49 N. Byrne, J. M. Pringle, C. Tiyapiboonchaiya, D. R. MacFarlane and M. Forsyth, The additive effect of zwitterion and nano-particles on ion dissociation in polyelectrolytes, *Electrochim. Acta*, 2005, **50**, 2733–2738.

50 N. Byrne, D. R. MacFarlane and M. Forsyth, Composition effects on ion transport in a polyelectrolyte gel with the addition of ion dissociators, *Electrochim. Acta*, 2005, **50**, 3917–3921.

51 M. E. Taylor and M. J. Panzer, Fully-Zwitterionic Polymer-Supported Ionogel Electrolytes Featuring a Hydrophobic Ionic Liquid, *J. Phys. Chem. B*, 2018, **122**, 8469–8476.

52 M. E. Taylor, D. Clarkson, S. G. Greenbaum and M. J. Panzer, Examining the Impact of Polyzwitterion Chemistry on Lithium Ion Transport in Ionogel Electrolytes, *ACS Appl. Polym. Mater.*, 2021, **3**, 2635–2645.

53 K. W. Wieck and M. J. Panzer, Ionogel Electrolytes Supported by Zwitterionic Copolymers Featuring Lithium Ion-Mediated, Noncovalent Cross-Links, *ACS Appl. Polym. Mater.*, 2023, **5**, 2887–2894.

54 X. Peng, H. Liu, Q. Yin, J. Wu, P. Chen, G. Zhang, G. Liu, C. Wu and Y. Xie, A zwitterionic gel electrolyte for efficient solid-state supercapacitors, *Nat. Commun.*, 2016, **7**, 1–8.

55 S. R. Wasserman, Y. T. Tao and G. M. Whitesides, Structure and reactivity of alkylsiloxane monolayers formed by reaction of alkyltrichlorosilanes on silicon substrates, *Langmuir*, 1989, **5**, 1074–1087.

56 H. Yan, Z. Chen, Y. Zheng, C. Newman, J. R. Quinn, F. Dötz, M. Kastler and A. Facchetti, A high-mobility electron-transporting polymer for printed transistors, *Nature*, 2009, **457**, 679–686.

57 M. Egginger, S. Bauer, R. Schwödiauer, H. Neugebauer and N. S. Sariciftci, Current versus gate voltage hysteresis in organic field effect transistors, *Monatsh. Chem.*, 2009, **140**, 735–750.

58 V. Georgiou, D. Veksler, J. P. Campbell, P. R. Shrestha, J. T. Ryan, D. E. Ioannou and K. P. Cheung, Ferroelectricity in Polar Polymer-Based FETs: A Hysteresis Analysis, *Adv. Funct. Mater.*, 2018, **28**, 1705250.

59 V. Coropceanu, J. Cornil, D. A. da Silva Filho, Y. Olivier, R. Silbey and J.-L. Brédas, Charge Transport in Organic Semiconductors, *Chem. Rev.*, 2007, **107**, 926–952.

60 R. Di Pietro, D. Fazzi, T. B. Kehoe and H. Sirringhaus, Spectroscopic Investigation of Oxygen- and Water-Induced Electron Trapping and Charge Transport Instabilities in n-type Polymer Semiconductors, *J. Am. Chem. Soc.*, 2012, **134**, 14877–14889.

61 S. Brixi, O. A. Melville, B. Mirka, Y. He, A. D. Hendsbee, H. Meng, Y. Li and B. H. Lessard, Air and temperature sensitivity of n-type polymer materials to meet and exceed the standard of N2200, *Sci. Rep.*, 2020, **10**, 4014.

62 H. Eyring, *Statistical Mechanics and Dynamics*, Wiley, 1964.

63 J. S. Harrison, D. A. Waldow, P. A. Cox, R. Giridharagopal, M. Adams, V. Richmond, S. Modahl, M. Longstaff, R. Zhuravlev and D. S. Ginger, Noncontact Imaging of Ion Dynamics in Polymer Electrolytes with Time-Resolved Electrostatic Force Microscopy, *ACS Nano*, 2019, **13**, 536–543.

64 A. Schönhals and F. Kremer, in *Broadband Dielectric Spectroscopy*, ed. F. Kremer and A. Schönhals, Springer, Berlin, Heidelberg, 2003, pp. 59–98.

65 G. Horowitz, M. E. Hajlaoui and R. Hajlaoui, Temperature and gate voltage dependence of hole mobility in polycrystalline oligothiophene thin film transistors, *J. Appl. Phys.*, 2000, **87**, 4456–4463.

66 M. Yoshizawa and H. Ohno, Anhydrous proton transport system based on zwitterionic liquid and HTFSI, *Chem. Commun.*, 2004, 1828–1829.

67 M. Yoshizawa, D. R. MacFarlane, M. Forsyth and H. Ohno, Zwitterionic Liquid/Acid Mixtures as Anhydrous Proton Conducting Systems, *Proc. Volcanol.*, 2004, **2004–24**, 73.

68 N. K. Jegatha, S. K. Hyung, K. L. Jae, B. W. Cho, J. R. Eun and S. G. Lee, Organic solvents containing zwitterion as electrolyte for Li ion cells, *Bull. Korean Chem. Soc.*, 2008, **29**, 1705–1710.

69 M. Hdidar, S. Chouikhi, A. Fattoum and M. Arous, Effect of hydrolysis degree and mass molecular weight on the structure and properties of PVA films, *Ionics*, 2017, **23**, 3125–3135.

© 2024 The Author(s). Published by the Royal Society of Chemistry

RSC Appl. Polym., 2024, **2**, 926–935 | **935**